Superweak Complexes of Tetrahedral P_4 Molecules with the Silver Cation of Weakly Coordinating Anions

Ingo Krossing*[a] and Leo van Wüllen[b]

Dedicated to Professor Hansgeorg Schnöckel on the occasion of his 60th birthday

Abstract: The silver aluminates $AgAl[OC(CF_3)_2(R)]_4$ (R = H, CH_3, CF_3) react with solutions of white phosphorus P_4 to give complexes that bind one or two almost undistorted tetrahedral P_4 molecules in an η^2 fashion: $[Ag(P_4)_2]^+[Al(OC(CF_3)_3)_4]^-$ (**1**) containing the first homoleptic metal–phosphorus cation, the molecular species $(P_4)AgAl[OC(CH_3)(CF_3)_2]_4$ (**2**), and the dimeric $Ag(\mu,\eta^2\text{-}P_4)Ag$ bridged $\{(P_4)AgAl[OC(H)(CF_3)_2]_4\}_2$ (**3**). Compounds **1**–**3** were characterized by variable-temperature (VT) ^{31}P NMR spectroscopy (**1** also by VT ^{31}P MAS-NMR spectroscopy), Raman spectroscopy, and single-crystal X-ray crystallography. Other Ag:P_4 ratios did not lead to new species, and this observation was rationalized on thermodynamic grounds. The $Ag(P_4)_2^+$ ion has an almost planar coordination environment around the Ag^+ ion due to $d_{x^2-y^2}(Ag) \rightarrow \sigma^*(P\text{—}P)$ backbonding. Calculations (HF-DFT) on six $Ag(P_4)_2^+$ isomers **4a**–**f** showed that the planar η^2 form **4a** is only slightly favored by 5.2 kJ mol^{-1} over the tetrahedral η^2 species **4b**; η^1-P_4 and η^3-P_4 complexes are less favorable (27–76 kJ mol^{-1}). The bonding of the P_4 moiety in $[RhCl(\eta^2\text{-}P_4)(PPh_3)_2]$, the only compound in which an η^2 bonding mode of a tetrahedral P_4 molecule has been claimed, must be regarded as a tetraphosphabicyclobutane, and not as a *tetrahedro*-P_4 complex, on the basis of the published NMR and vibrational spectra, the calculated geometry of $[RhCl(P_4)(PH_3)_2]$ (**10**), the highly endothermic (385 kJ mol^{-1}) calculated dissociation enthalpy of **10** into P_4 and $RhCl(PH_3)_2$ (**11**), as well as atoms in molecules (AIM) and natural bond orbital (NBO) population analyses of **10** and the $Ag(P_4)_2^+$ ion. Therefore, **1**–**3** are the first examples of species containing η^2-coordinated tetrahedral P_4 molecules.

Keywords: density functional calculations · phosphorus · silver · weakly coordinating anions

Introduction

Owing to the unique structure and unusual bonding of the tetrahedral tetraphosphorus molecule, its chemistry has attracted much attention over the past decades. However, knowledge on species containing *tetrahedro*-P_4 is still very limited. Recently complexes of P_4 with H^+,[1] Li^+,[2] or Ag^+[3] were investigated by mass spectrometry, and on the basis of quantum-chemical investigations it was concluded that the P_4 molecule retains its structural integrity when complexed with Li^+ but forms a P-H-P three-center, two-electron bond in HP_4^+. Few structures in which tetrahedral P_4 molecules are coordinated to transition metal fragments are known,[4, 5] and the question whether η^2 complexes are derived from neutral *tetrahedro*-P_4 or from P_4^{2-} in a tetraphosphabicyclobutane structure is still disputed. For example, $[Rh^ICl(\eta^2\text{-}P_4)(PPh_3)_2]$[4b] can formally be viewed as a $Rh^{III}(P_4^{2-})$ complex.[4c] In fact, upon reaction with transition metal fragments, decomposition of the tetrahedral P_4 molecule is usually observed, and phosphidic degradation appears to be the normal reaction pathway of P_4.[6] This led to the question whether very weak and simple complexes between a univalent metal cation such as Ag^+[7] and the P_4 molecule could also be accessible in condensed phases. Such compounds can be regarded as initial steps on the usual pathway leading to phosphidic degradation of P_4.[6,7]

Here we report on the preparation and structural characterization of three silver–P_4 complexes containing one or two almost undistorted tetrahedral P_4 moieties: $[Ag(P_4)_2]^+[Al(OC(CF_3)_3)_4]^-$ (**1**) containing the first homoleptic metal–P_4 cation, the molecular species $(P_4)AgAl[OC(CH_3)(CF_3)_2]_4$ (**2**) and the dimeric $Ag(\mu,\eta^2\text{-}P_4)Ag$ bridged $[\{(P_4)AgAl[OC(H)(CF_3)_2]_4\}_2]$ (**3**). A preliminary account on the $Ag(P_4)_2^+$

[a] Dr. I. Krossing
Universität Karlsruhe, Institut für Anorganische Chemie
Engesserstrasse Geb. 30.45, 76128 Karlsruhe (Germany)
Fax: (+49) 721 608 48 54
E-mail: krossing@achpc9.chemie.uni-karlsruhe.de

[b] Dr. L. van Wüllen[+]
Max-Planck Institut für Festkörperchemie
Heisenbergstrasse 1, 70569 Stuttgart (Germany)

[+] Solid-state NMR spectroscopy.

Supporting information for this article is available on the WWW under http://www.wiley-vch.de/home/chemistry/ or from the author.

  0947-6539/02/0803-0700 $ 17.50+.50/0

ion has been given.[8] For the stabilization of these superweak silver–phosphorus complexes weakly coordinating anions (WCAs) of the type $Al(OR_F)_4^-$ (OR_F = polyfluoroalkoxy) had to be used as spectator anions.[9] Moreover we reinterpret the bonding of the $Rh(P_4)$ moiety in $[RhCl(P_4)(PPh_3)_2]$ as a tetraphosphabicyclobutane P_4 unit, and not as a molecular *tetrahedro*-P_4 complex, on the basis of the published NMR and vibrational spectra, the calculated geometry and thermochemistry of $[RhCl(P_4)(PH_3)_2]$ (**10**), as well as AIM and NBO population analyses of **10** and the $Ag(P_4)_2^+$ ion.

Results and Discussion

Syntheses and NMR spectroscopic characterization: Initial attempts to prepare $M^+(P_4)$ complexes were performed by treating $LiAl(OR_F)_4$ with white phosphorus alone or in solvents such as CH_2Cl_2 and 1,2-$Cl_2C_2H_4$. However, NMR spectroscopy indicated the failure of these reactions, and we therefore replaced the hard Lewis acid Li^+ by the soft Ag^+ (P_4 is a soft Lewis base). Analogously, the weak but soft Lewis bases Se_6 and S_8 formed stable complexes with $Ag[Sb(OTeF_5)_6]$.[10] Several Ag^+:P_4 ratios between 1:1 and 1:4 were used, but for each anion a preferred product **1**, **2**, or **3** always crystallized from the mixture (see Scheme 1).

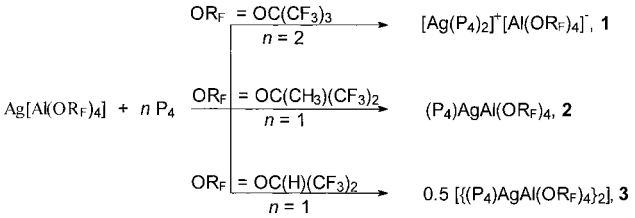

Scheme 1. Reactions leading to the Ag–P_4 adducts **1**–**3**.

The nature of **1**–**3** was established by Raman and NMR spectroscopy and by single-crystal X-ray crystallography. All three compounds are colorless, highly soluble in CH_2Cl_2, $CHCl_3$, and 1,2-$Cl_2C_2H_4$, and ignite spontaneously in air. The molecular species **2** and **3** are also soluble in CS_2 and *n*-pentane, and therefore dissociation into discrete $Ag(P_4)^+$ ions and $Al(OR_F)_4^-$ ions in solution appears unlikely. In the room-temperature ^{31}P NMR spectra of **1**–**3** the chemical shift of the P_4 molecule is only very slightly shifted to lower field and occurs as a sharp singlet ($\delta(^{31}P) = -522$ (P_4), -497 (**1**), -515 (**2**), -514 (**3**) in CD_2Cl_2). The room-temperature solid-state ^{31}P MAS-NMR spectrum of **1** showed essentially the same shift ($\delta(^{31}P) = -511$ at 298 and -507 at 154 K; Figure 1).

The VT ^{31}P MAS-NMR spectra presented in Figure 1 clearly reflect the motion of the P_4 tetrahedron. The very small overall linewidth of the room-temperature spectrum is consistent with a rotation of the P_4 tetrahedron about all C_3 axes, achieved by intermediate η^1 coordination as in Equation (1a). Upon lowering the temperature, the characteristic frequency is reduced until it matches the MAS frequency at 180 K. Here the interference of the macroscopic rotation (MAS) and the microscopic internal P_4 reorientation leads to disappearance of the NMR signal. Further decrease of the temperature freezes the rotation of P_4 about the C_3 axes, and the spectra exhibit the full chemical shift anisotropy (CSA) pattern, as indicated by the numerous spinning side bands. The isotropic chemical shift remains virtually constant at $\delta = -511$ at room temperature and -507 at 154 K. This is in agreement with the order–disorder phase transition observed by X-ray crystallography (see below). The chemical shift of $\delta = -511$ for **1** in the solid state at room temperature suggests that the ^{31}P NMR chemical shift of **1** is due to a fast equilibrium between several $Ag(P_4)_2^+$ isomers and only to a small extent, if at all, to a fast equilibrium between $Ag(P_4)_2^+$, P_4, and Ag^+.[11] By analogy the same holds for **2** and **3**. A similar conclusion was drawn from the calculated ^{31}P NMR shifts of $Ag(P_4)_2^+$ and $Ag(P_4)^+$ below. We note that available ^{31}P NMR signals of species containing coordinated P_4 moieties are usually shifted considerably to lower field; for example, $\delta = -282$ (av) in $[RhCl(\eta^2\text{-}P_4)(PPh_3)_2]$,[4b] -391 (1P) and -489 (3P) in $[Re(CO)_2(\eta^1\text{-}P_4)(triphos)]^+$,[4d] and -422 (1P) and -473 (3P) in $[W(CO)_3(\eta^1\text{-}P_4)\{P(C_6H_{11})_3\}]$.[4c] Recording the ^{31}P NMR spectra of **1** and **3** at low temperature led to a small shift to lower field ($\Delta\delta = 10-11$ at $-100\,^\circ C$) and to line broadening, but no evidence for an AB_3 or A_2B_2 spin system was found, in agreement with a fluxional system. Ab initio calculations (see below) showed that the calculated gauge invariant atomic orbitals (GIAO) ^{31}P NMR shifts of the two nonequivalent phosphorus atoms in four $Ag(P_4)_2^+$ isomers **4a**–**d** only differ by $\Delta\delta = 11-16$ (see Table 1). Experimentally, the two lines are indistinguishable on the NMR timescale, and prevents assignment of a unique solution structure of the $Ag(P_4)_2^+$ ion. Probably a mixture of **4a**–**d** will be present in solution [Eq. (1a)].

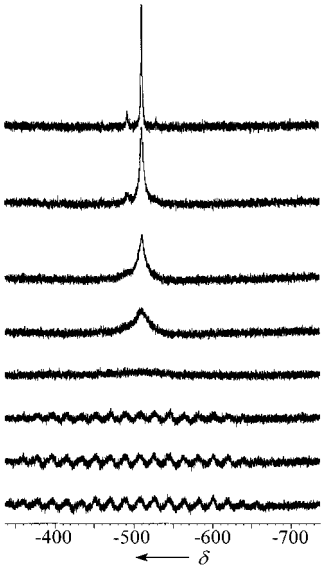

Figure 1. Solid-state ^{31}P MAS-NMR spectrum of **1** with 3 kHz spinning frequency at 298 (top), 270, 240, 210, 180, 170, 160, and 154 K (bottom).

$$Ag(\eta^2\text{-}P_4)_2^+ (\mathbf{4a,b}) \rightleftharpoons (\eta^1\text{-}P_4)Ag(\eta^2\text{-}P_4)^+ \rightleftharpoons Ag(\eta^1\text{-}P_4)_2^+ (\mathbf{4c,d}) \quad (1a)$$

In the η^1 mode, rotation around the Ag–P axis is presumably very fast and thus equilibrium (1a) makes all phosphorus atoms equivalent on the timescale of solution and

Table 1. Calculated GIAO ^{31}P NMR shifts and relative energies of several $Ag(P_4)_2^+$ and $Ag(P_4)^+$ isomers in the gas phase and in CH_2Cl_2 solution (in parentheses).

Species	$\delta(^{31}P)$(coord.) [ppm]	$\delta(^{31}P)$(non coord.) [ppm]	$E_{rel.}$ [kJ mol^{-1}]
$Ag(P_4)_2^+$ **4a** (η^2; D_{2h})	−507	−518	0
$Ag(P_4)_2^+$ **4b** (η^2; D_{2d})	−501	−517	+5
$Ag(P_4)_2^+$ **4c** (η^1; D_{3h})	−499	−512	+27
$Ag(P_4)_2^+$ **4d** (η^1; D_{3d})	−500	−512	+27
$Ag(P_4)_2^+$ **4e** (η^3; D_{3h})	−550	−632	+72
$Ag(P_4)_2^+$ **4f** (η^3; D_{3d})	−551	−632	+75
$Ag(P_4)^+$ **5** (η^2; C_{2v})	−504	−508	0 (0)[a]
$Ag(P_4)^+$ **5a** (η^1; C_{3v})	−461	−516	+24 (+0.6)[a]
$Ag(P_4)^+$ **5b** (η^3; C_{3v})	−570	−664	+30 (−)[b]

[a] COSMO-model. [b] Calculation did not converge.

MAS-NMR spectroscopy. However, η^3 coordination as in **4e**,**f** can be excluded on the basis of the calculated shifts and the high relative energies (Table 1). Owing to the similarity of calculated and observed ^{31}P NMR chemical shifts we conclude that the majority of the $Ag(P_4)_2^+$ and (anion)$Ag(P_4)$ complexes in **1** and **3** remain as η^2 and η^1 complexes in solution and dissociate only slightly into Ag^+ and P_4. However, in none of the spectra at all temperatures and with all $Ag:P_4$ ratios tested the signal of free P_4 was visible.[12] In **3** the exchange of the coordinated P_4 molecules may occur via a dimeric structure like that observed in the solid state (see below and Eq. (1b), $R = C(H)(CF_3)_2$).

$$2\,(P_4)Ag[Al(OR)_4] \rightleftharpoons \{(P_4)Ag[Al(OR)_4]\}_2 \rightleftharpoons 2\,(P_4)Ag[Al(OR)_4] \quad (1b)$$

However, these exchange processes are faster than the NMR timescale even at −100 °C and therefore lead to the relatively simple one-line spectra. Equations (1a) and (1b) were supported by a systematic VT ^{31}P NMR spectroscopic investigation of the properties of CD_2Cl_2 solutions with $Ag^+:P_4$ ratios of 1.0:1.0–2.5 for $R = C(H)(CF_3)_2$ and 1.0:2.0–4.0 for $R = C(CF_3)_3$.[12]

A different situation was encountered for **2**, which contains the most basic anion of this $Al(OR_F)_4^-$ series.[9] The P_4 molecule of **2** is the most weakly bound amongst **1**–**3**.[13] Upon cooling a sample of **2** in CD_2Cl_2, two broad lines in a ratio of 1:7 at $\delta(^{31}P) = -466$ and −518, as well as a sharp line attributable to $Ag(P_4)_2^+$, appeared at −80 °C and were the dominant signals at −90 °C (Figure 2).

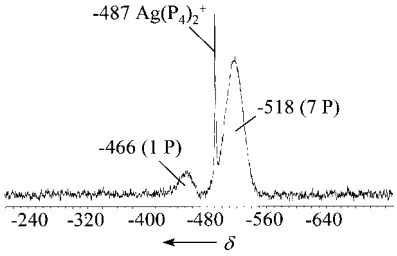

Figure 2. ^{31}P NMR spectrum of **2** in CD_2Cl_2 at −90 °C.

Comparison with the calculated GIAO ^{31}P NMR shifts of three $Ag(P_4)^+$ isomers **5**, **5a**, and **5b** (Table 1) that served as models for (anion)$Ag(P_4)$, which is presumably a molecular compound in solution, shows that this is best understood as a 1:1 mixture of $Ag(\eta^1\text{-}P_4)$ and $Ag(\eta^2\text{-}P_4)$ moieties within the (anion)$Ag(P_4)$ structure [Eq. (2a), $R = C(CH_3)(CF_3)_2$], with a small amount of $Ag[Al(OR)_4]$ and $Ag(P_4)_2[Al(OR)_4]$ (sharp line at $\delta = -487$, cf. $\delta(^{31}P)$ (**1**, −90 °C) = −488 and $\delta(^{31}P)$ (P_4, −80 °C) = −516[12]) also present [Eq. (2b)].

$$(\eta^2\text{-}P_4)Ag[Al(OR)_4] \rightleftharpoons (\eta^1\text{-}P_4)Ag[Al(OR)_4] \quad (2a)$$

$$2\,(P_4)Ag[Al(OR)_4] \rightleftharpoons Ag(P_4)_2[Al(OR)_4] + Ag[Al(OR)_4] \quad (2b)$$

The broad signal at $\delta(^{31}P) = -466$ is due to the only coordinated P atom of the η^1 species (calcd: $\delta = -461$) and the more intense signal at $\delta = -518$ is due to a superposition of the signals for the three basal P atoms of the η^1 species and all the phosphorus atoms of the η^2 form (see Table 1). In the gas phase the η^1 form in the $Ag(P_4)^+$ model is 24 kJ mol^{-1} less stable than the η^2 form, which is compensated in CH_2Cl_2 solution by the 23.4 kJ mol^{-1} higher solvation energy of the η^1 isomer (COSMO model: $\Delta G_{solv} = -171.4$ kJ mol^{-1} for **5**, −194.8 kJ mol^{-1} for **5a**). This accounts for the 1:1 mixture observed by NMR spectroscopy. Based on the calculated NMR shifts, the η^3 isomer is ruled out and certainly plays no role in solution.

Reactions of 1 with the Lewis bases C_6D_6, 1,5-cyclooctadiene, and S_8: When **1** was dissolved in C_6D_6, the room-temperature ^{31}P NMR spectrum showed one sharp signal at $\delta = -520$, that is, the chemical shift of free P_4 in this solvent. Therefore, we conclude that the $Ag(P_4)_2^+$ complex is destroyed in C_6D_6, and an $Ag(C_6D_6)_n^+$ ($n \approx 2$) complex and $2\,P_4$ are formed. This is consistent with the many known stable crystalline Ag^+ arene complexes.[9, 14] Similarly, we also observed destruction of the $Ag(P_4)_2^+$ complex when two equivalents of 1,5-cyclooctadiene (COD) were added to a solution of **1** in $CDCl_3$ ($\delta^{31}P = -521$ (free P_4); an $[Ag(cod)_2]^+BF_4^-$ (cod = 1,5-cyclooctadiene) salt is known[15]). However, octasulfur S_8 is an even weaker donor than P_4; an NMR-scale reaction between **1** and two equivalents of S_8 in $CDCl_3$ with ultrasonic enhancement for 30 min left the sulfur unconverted at the bottom of the NMR tube. The ^{31}P NMR spectrum of this mixture showed only one line at $\delta^{31}P = -496$, that is, exactly the position of **1** in this solvent. Under the same conditions, $Ag[Al(OC(CF_3)_3)_4]$ reacted quantitatively with two equivalents of S_8 to give $Ag(S_8)_2$-$[Al(OC(CF_3)_3)_4]$.[16]

Crystal structures: Crystallographic and refinement data of **1**–**3** are collected in Table 5.

Overall structure: The solid-state structures of **1**–**3** contain side-on-bonded $Ag(\eta^2\text{-}P_4)$ moieties with comparable structural parameters (Table 2). However, **1**, which contains the least basic anion,[9] is a salt, and the Ag atom binds two tetrahedral P_4 molecules so that the local coordination sphere of the Ag atom is nearly planar and the two AgP_2 planes are tilted by only 10.6° (Figure 3).

When the data for **1** were collected at 200 K, an order–disorder phase transition occurred, and the $Ag(P_4)_2^+$ ion became perfectly D_{2h}-symmetric, while all $OC(CF_3)_3$ groups of the $Al(OC(CF_3)_3)_4^-$ ion were disordered and freely rotating (Figure 4).[17] Therefore, the D_{2h} conformation should be the

  0947-6539/02/0803-0702 $ 17.50+.50/0 *Chem. Eur. J.* **2002**, *8*, No. 3

Table 2. Structural parameters of the Ag(η^2-P_4) moieties in **1**–**3**.

Parameter[a]	1	2	3
d(Ag–P) range [Å]	2.536(1)–2.548(1)	2.5262(8)–2.5274(9)	2.512(2)–2.523(2)
d(Ag–P) av [Å]	2.541(1)	2.5268(9)	2.519(2)
d(a) range [Å]	2.328(2)–2.330(2)	2.3076(12)	2.317(2)–2.334(2)
d(a) av [Å]	2.329(2)	–	2.326(2)
d(b) range [Å]	2.145(2)–2.163(2)	2.152(1)–2.174(1)	2.151(2)–2.174(2)
d(b) av [Å]	2.154(2)	2.159(1)	2.160(2)
d(c) range [Å]	2.172(2)–2.174(2)	2.188(2)	2.161(2)–2.177(2)
d(c) av [Å]	2.173(2)	–	2.169(2)
P-P-P range [°]	56.89(7)–65.53(7)	57.29(4)–64.48(4)	56.92(7)–65.26(6)

[a] a, b, c refer to the distances shown in **A**.

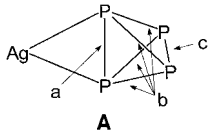

A

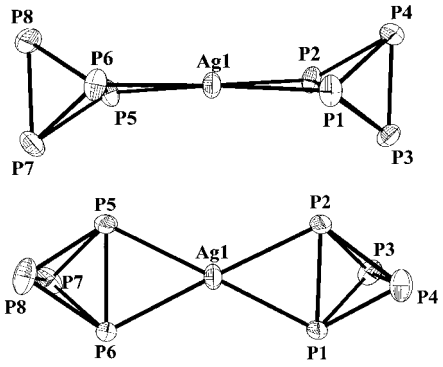

Figure 3. The solid-state structure of the $Ag(P_4)_2^+$ ion in **1** at 150 K. Thermal ellipsoids are drawn at the 25% probability level; for clarity the $Al(OC(CF_3)_3)_4^-$ ion is omitted.

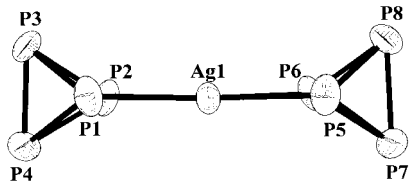

Figure 4. The solid-state structure of the $Ag(P_4)_2^+$ ion in **1** at 200 K. Thermal ellipsoids are drawn at the 25% probability level; for clarity the disordered $Al(OC(CF_3)_3)_4^-$ ion is omitted. The bond lengths and angles are similar to those in the low-temperature modification.[17]

ground state and is not induced by cation–anion contacts. At 150 K, the rotation of the CF_3 groups is hindered by the formation of eleven weak P–F contacts at 3.12–3.36 Å (Figure 5, sum of van der Waals radii for P and F: 3.40 Å), and these weak interactions slightly distort the D_{2h} conformation.

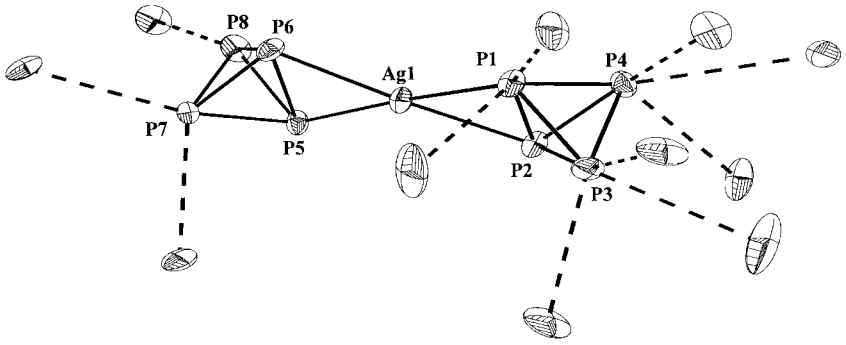

Figure 5. Stabilizing P···F contacts in the low-temperature modification of **1**.

There is only one family of ions with an isolobal topology to **1**, namely, $[M\{M'(tppme)(P_3)\}_2]PF_6$ (M = Cu, Au; M′ = Co, Rh, Ir; tppme = 1,1,1-tris(diphenylphosphanylmethyl)ethane), in which the local coordination of the M atom is between planar and tetrahedral [the two MP_2 planes form an angle of about 51° (Au) or 57° (Cu); in **1**: 10.6° (150 K) or 0° (200 K)].[18] In contrast to **1**, the Ag^+ ions in **2** and **3** are additionally ligated by the $Al[OC(R)(CF_3)_2]_4^-$ ions (R = H, CH_3), and Ag^+ can therefore only bind one P_4 molecule. The oxygen atoms of these anions are sterically more accessible and more basic than those in $Al[OC(CF_3)_3]_4^-$[9] and thus also coordinate in a bidentate fashion to the Ag atom to give the molecular species **2** (Ag–O 2.365(2), 2.388(2) Å; Figure 6) and the dimeric species **3** (Ag–O 2.353(3)–2.401(3) Å; Figure 7). The latter distances are comparable to those of other

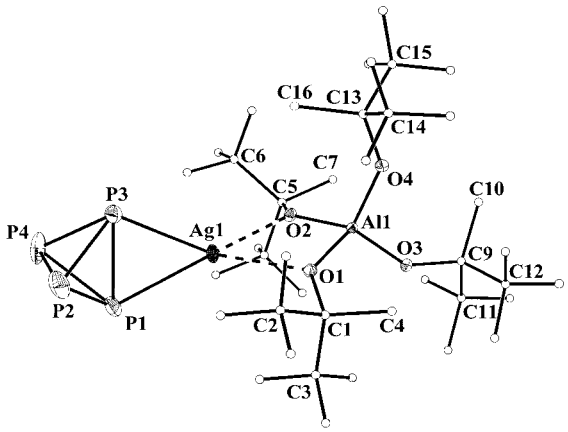

Figure 6. The solid-state structure of **2**. Thermal ellipsoids are drawn at the 25% probability level; for clarity all hydrogen atoms are omitted, and carbon and fluorine (gray) atoms are shown as small circles on an arbitrary scale.

weak Ag–O interactions, for example, in $(OC)Ag[B(OTeF_5)_4$ (Ag–O 2.324(6), 2.436(6) Å).[19] Interestingly, the local AgO_2P_2 coordination sphere in **2** is tetrahedral, while that in **3** is planar. However, the two $(P_4)AgAl[OC(H)(CF_3)_2]_4$ units in **3** dimerize by weak Ag–P contacts of 3.352(2)–3.429(2) Å, and if one weak Ag–F interaction per Ag atom (3.250(3) and 3.282(3) Å) is included, the local coordination environment of the silver atoms is elongated octahedral (Figure 8). In contrast to **3**, no Ag–F contact below 4.269 Å is found in **2**. The phosphorus atoms in **2** (**3**) exhibit three (five) weak stabilizing contacts to fluorine atoms below the sum of the respective van der Waals radii of 3.40 Å: 3.302(1) to P3, 3.350(1) to P2, and 3.400(1) Å to P1 (**3:** 3.230(3) to P4, 3.301(3) to P1, 3.328(3) to P2, 3.331(3) to P7, and 3.340(3) Å to P6).

The Ag(η^2-P_4) moieties: All three solid-state structures contain Ag(η^2-P_4) moieties with local C_{2v}

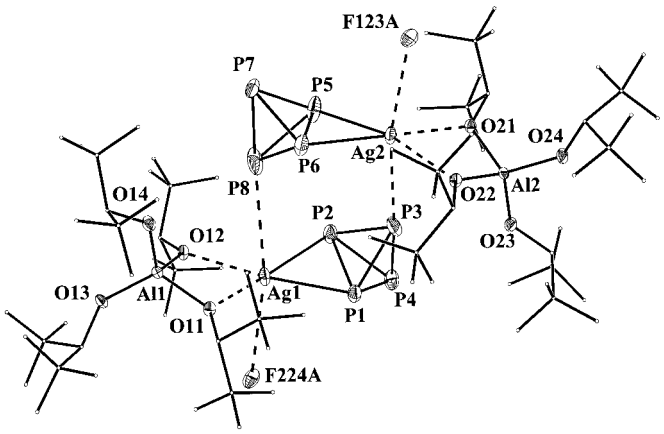

Figure 7. The dimeric solid-state structure of **3**. Thermal ellipsoids are drawn at the 25% probability level; for clarity all hydrogen atoms are omitted, and carbon and fluorine atoms (apart from F123A and F224A) are shown as small circles on an arbitrary scale.

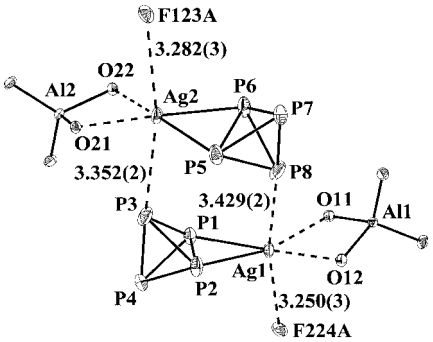

Figure 8. The local octahedral coordination of the Ag atoms in **3**, including one weak Ag–F contact each. All hydrogen, carbon, and fluorine atoms except for F123A and F224A are omitted for clarity.

symmetry. The Ag–P [P–P] distances vary only slightly and range from 2.519 (**3**) to 2.541 Å (**1**) (2.145 (**1**) to 2.334 Å (**3**)). The coordinated edge of the P_4 tetrahedron is elongated by about 0.10–0.12 Å, but all other P–P distances are shortened by 0.02 to 0.07 Å relative to the free P_4 molecule (2.21 Å; see Table 2). There are three sets of distinctly different P–P bond lengths: the coordinated edge (av 2.323 Å, denoted a), the four adjacent bonds (av 2.158 Å, b) and the opposite edge (av 2.177 Å, c), but the overall geometry of the P_4 molecule is only slightly distorted, as seen by the small range of P-P-P bond angles of 56.9–65.5°. In contrast, the coordinated edge in $[RhCl(\eta^2\text{-}P_4)(PPh_3)_2]$[4b] is elongated to 2.462(2) Å, that is, 0.25 Å longer than in P_4. The Rh–P_4 bonds in the complex are short (av 2.293 Å, cf. av 2.529 Å in **1**–**3**), even shorter than the strong dative Rh–PPh_3 bonds in the same molecule (av 2.333 Å). This is surprising given the low nucleophilicity of the neutral P_4 molecule, and one would expect a difference of about 0.1 Å between Ag–P and Rh–P bonds, since the atomic and ionic radii of silver and rhodium differ by this amount, whereas the difference between **1**–**3** and $[RhCl(\eta^2\text{-}P_4)(PPh_3)_2]$ is about 0.23 Å.[4b] This again underlines the weak coordination of the tetrahedral P_4 molecule in **1**–**3** and raises the question whether the P_4 moiety in $[RhCl(\eta^2\text{-}P_4)(PPh_3)_2]$[4b] should better be formulated as being formally derived from P_4^{2-}.

Raman spectra: The FT-Raman spectra of **1**–**3** also show the weak coordination to the Ag^+ ion. Upon coordination of P_4 the local symmetry of the $Ag(P_4)$ moieties is lowered from T_d (in P_4) to C_{2v}, and therefore the three A_1, T_2, and E Raman bands of P_4 split into six Raman active A_1 (3), A_2 (1), B_1 (1), and B_2 (1) modes. All observed frequencies of **1**–**3** are collected in Table 3, and a typical spectrum (of **1**) is shown in Figure 9.

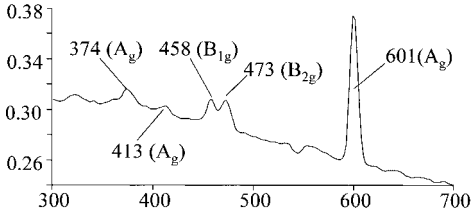

Figure 9. FT-Raman spectrum of **1** between 300 and 700 cm^{-1}.

The Raman frequencies of **1**–**3** are very similar and only slightly shifted relative to those of P_4; this indicates nearly undistorted and therefore weak coordination of the P_4 molecule. In contrast, the P–P Raman frequencies of $[RhCl(\eta^2\text{-}P_4)(PPh_3)_2]$ are shifted to lower energy by 27–72 cm^{-1}, in agreement with considerable weakening of the P–P bonds and strong coordination to the rhodium center. Moreover, the symmetric A_1 breathing mode of P_4, which in free P_4 and **1**–**3** is the most intense band, is weak in $[RhCl(\eta^2\text{-}P_4)(PPh_3)_2]$.[4b] This again raises the question of whether this η^2-P_4 moiety should be regarded as neutral P_4 or P_4^{2-}.

Calculations: To understand the bonding situation in the $Ag(\eta^2\text{-}P_4)$ moieties in **1**–**3** and to establish the thermodynamics of **1**–**3** we fully optimized the structures of six isomers of $Ag(P_4)_2^+$ (η^2-D_{2h} (**4a**), η^2-D_{2d} (**4b**), η^1-D_{3h} (**4c**), η^1-D_{3d} (**4d**),

Table 3. Experimental Raman spectra of **1**–**3**, calculated scaled[20] frequencies ν_{calcd} of $Ag(P_4)_2^+$ (D_{2h}), (**4a**), and $(P_4)AgAl(OCF_3)_2F_2$ (C_2) (**6a**), experimental frequencies ν_{exp} of P_4 and $[RhCl(\eta^2\text{-}P_4)(PPh_3)_2]$[4b] [in cm^{-1}].

1 ν_{exp} (I%)	**2** ν_{exp} (I%)	**3** ν_{exp} (I%)	$Ag(P_4)_2^+$ ν_{calcd} (I%) sym.	**6a** ν_{calcd} (I%) sym.	$Rh(P_4)$[a] ν_{exp} (I%)	P_4[b] ν_{exp} (I%) sym.
601 (100)	598 (100)	598 (100)	595 (100) A_g	596 (100) A_1	571 (w)	598 (100) A_1
473 (18)	469 (sh)	471 (26)	468 (21), B_{2g}	470 (28) B_1	438 (m)	
458 (16)	457 (29)	459 (sh)	465 (13), B_{1g}	469 (19) B_2	386 (m)	457 (37) T_2
413 (5)	414 (7)	414 (8)	413 (15), A_g	414 (21) A_1	374 (sh)	
381 (sh)	371 (6)	374 (12)	366 (7), B_{3g}	367 (13) A_2	344 (w)	360 (9) E
374 (9)	358 (6)	–	361 (12), A_g	362 (20) A_1		

[a] Rh = $Rh(PPh_3)_2(Cl)$. [b] In the solid state on our spectrometer.

0947-6539/02/0803-0704 $ 17.50+.50/0 *Chem. Eur. J.* **2002**, *8*, No. 3

η^3-D_{3h} (**4e**), η^3-D_{3d} (**4f**)), $Ag(P_4)^+$ (C_{2v}, **5**), two isomers of $(P_4)AgAl(OCF_3)_2F_2$ (C_2 tetrahedral (**6a**), C_{2v} planar (**6b**)), $AgAl(OCF_3)_2F_2$ (C_2, **7**), $Al(OCF_3)_2F_2^-$ (C_2, **8**), and P_4 (T_d, **9**) at the hybrid HF-DFT MPW1PW91 level. The OCF_3 and F ligands served as models for the fluorinated alkoxy ligands in the aluminate anions of **2** and **3**. All optimized geometries of **4a**, **5**–**8** (Figure 10) are in very good agreement with the structural parameters of **1**–**3** or other comparable species and are therefore not discussed in detail.

The optimized geometry of P_4 has a P–P bond length of 2.209 Å (exp: 2.21 Å) and a total energy of –1365.48801 a.u. The tetrahedrally coordinated compound **6a** is a true minimum, but the planar species **6b** is a fifth-order saddle point with small imaginary frequencies of $7i$–$28i$ cm^{-1}. However, the fact that **6a** is only favored by 15 kJ mol^{-1} over **6b** indicates the presence of a very shallow hypersurface for compound **6**. A similar situation to that in **6a**,**b** is encountered for the $Ag(P_4)_2^+$ cation (**4**): The tetrahedrally coordinated cation **4b** is a second-order saddle point but is only 5.2 kJ mol^{-1} less favorable than the planar global minimum **4a**. All other η^1- and η^3-bonded species **4c**–**f** are also saddle points and are about 27 (η^1) to 76 kJ mol^{-1} (η^3) less favorable than **4a** (for geometries and total energies of **4b**–**f**, see Supporting Information). All calculated imaginary frequencies of **4b**–**f** are very small ($<44i$ cm^{-1}) and therefore indicate shallow potential energy wells on the hypersurface of **4**.

To compare the η^2 bonding of the P_4 molecules of **1**–**3** to that of $[RhCl(\eta^2\text{-}P_4)(PPh_3)_2]$[4b] and to answer the question whether the Rh atom in this species should be regarded as Rh^I or Rh^{III} (formally with a P_4^{2-} ligand), we fully optimized the model compounds $[RhCl(\eta^2\text{-}P_4)(PH_3)_2]$ (**10**) and $[RhCl(PH_3)_2]$ (**11**) at the same level of theory as **4**–**9**. The structural features of $[RhCl(\eta^2\text{-}P_4)(PPh_3)_2]$[4b] are reproduced in the optimized structure of **10** (Figure 11) within 0.034 Å and thus lend credibility to the results of the calculation (calculated structural features of **11** are given in the Supporting Information).

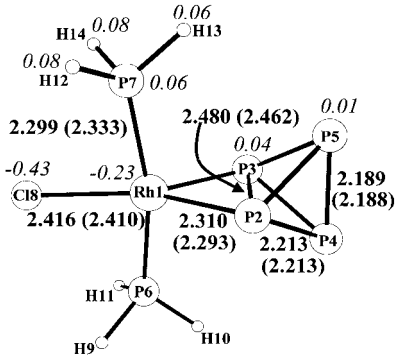

10 (C_1); -7176.97176 a.u.

Figure 11. Optimized geometry and structural parameters of $[RhCl(\eta^2\text{-}P_4)(PH_3)_2]$ (**10**). The corresponding bond lengths of the structurally characterized $[RhCl(\eta^2\text{-}P_4)(PPh_3)_2]$[4b] are given in parentheses, and calculated Mulliken charges in italics.

Thermodynamics of the tetraphosphorus complexes: We quantified the weak coordination behavior in complexes **1**–**3** with the help of model reactions in comparison with $[RhCl(\eta^2\text{-}P_4)(PH_3)_2]$ (**10**) and rationalized the exclusive formation of the molecules **2** and **3** and the salt **1**. Suitable Born–Fajans–Haber cycles were constructed to approximate

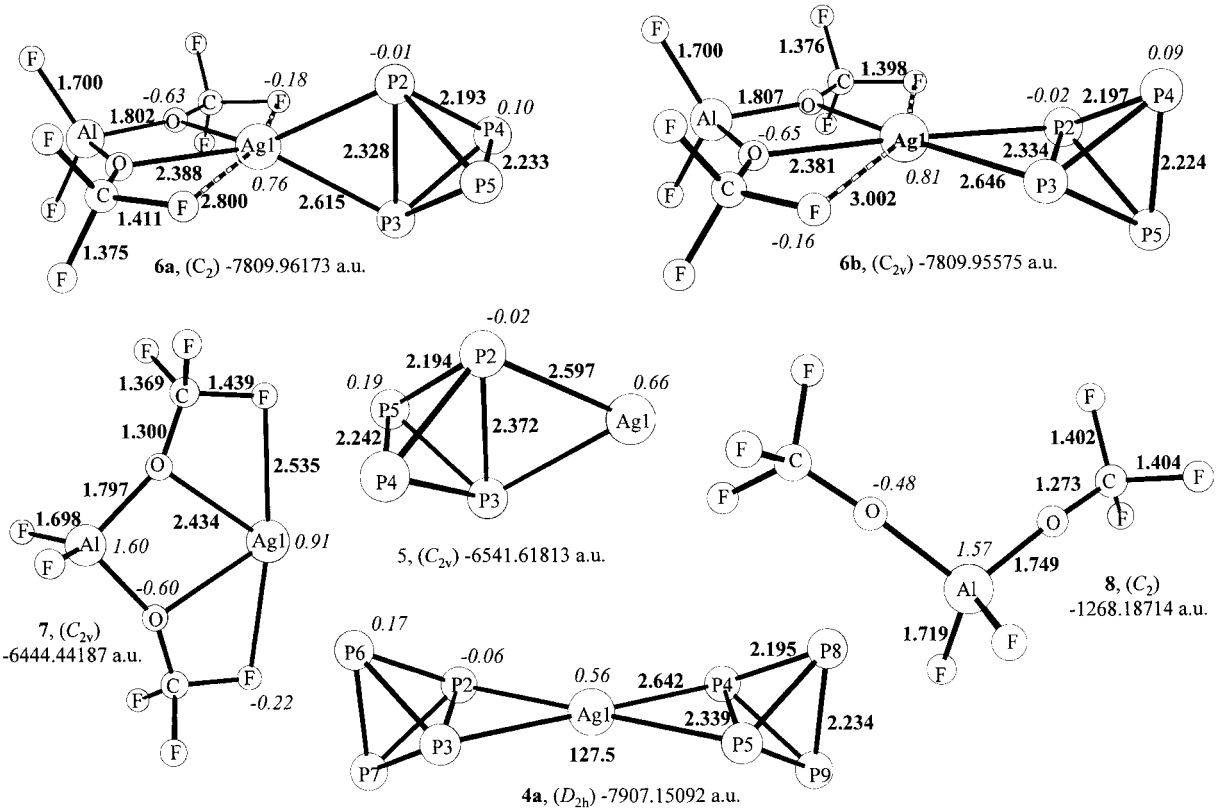

Figure 10. Optimized geometries of **4a**, **5**–**8** at the MPW1PW91 level; selected calculated Mulliken charges are given in italics.

the solid-state behavior. The lattice potential enthalpies of salts were estimated by the modified Kapustinskii equation of Jenkins and Passmore,[21] and the sublimation enthalpies of molecules by a recently employed formula.[9] All estimated lattice potential enthalpies and sublimation enthalpies can be found in the Supporting Information. Estimated solid-state enthalpies of reaction should be accurate to within 30 kJ mol^{-1},[22] while the gas-phase values calculated by hybrid HF-DFT methods should be correct to within 20 kJ mol^{-1}.[23]

The strength of coordination of the tetraphosphorus molecule: The dissociation of the model complex $(P_4)AgAl(OCF_3)_2F_2$ (**6a**) into P_4 and $AgAl(OCF_3)_2F_2$ (**7**) [Eq. (3)] was calculated to be endothermic (endergonic) only by 91 (14) kJ mol^{-1}. Similarly the first step of the dissociation of $Ag(P_4)_2^+$ (**4a**) into **5** and P_4 is endothermic (endergonic) by only 112 (61) kJ mol^{-1} [Eq. (4)].[24] In contrast, the P_4 molecule in the model compound $[RhCl(\eta^2\text{-}P_4)(PH_3)_2]$ (**10**), calculated at the same level, is bonded much more strongly, and dissociation of **10** is highly endothermic (endergonic) by 385 (334) kJ mol^{-1} [Eq. (5)].

$$(P_4)AgAl(OCF_3)_2F_2(g) \longrightarrow P_4(g) + AgAl(OCF_3)_2F_2(g) \quad (3)$$

$$Ag(P_4)_2^+(g) \longrightarrow P_4(g) + Ag(P_4)^+(g) \quad (4)$$

$$[RhCl(P_4)(PH_3)_2](g) \longrightarrow P_4(g) + Rh(PH_3)_2Cl(g) \quad (5)$$

Taking the calculated gas-phase reaction enthalpy of Equation (3) as a rough approximation of the expected gas-phase enthalpies of dissociation of **2** and **3** and modeling the solid-state enthalpies of dissociation of **2** and **3** by incluing the respective sublimation enthalpies, we estimate that the dissociation into the solid silver compound and solid neutral P_4 is only endothermic by 68 kJ mol^{-1} [Eq. (6); R = H, CH_3].[22]

$$(P_4)AgAl[OC(R)(CF_3)]_4(s) \longrightarrow P_4(s) + AgAl[OC(R)(CF_3)]_4(s) \quad (6)$$

Equations (3), (4), and (5) clearly demonstrate the weak coordination of the P_4 molecule to the Ag^+ ion in **1**–**3**, while Equation (5) indicates that the P_4 moiety in **10** is strongly bonded to the rhodium center, so that dissociation into neutral P_4 and $Rh(PH_3)_2Cl$ is very unfavorable.

*Should species other than **1**–**3** be accessible?* The experiment showed that, regardless of the Ag:P_4 ratio, only one P_4-containing species crystallized from the reaction mixture for each silver salt. This raised the question whether the $Ag(P_4)_2^+$ ion is stable with a $Al[OC(R)(CF_3)]_4^-$ ion (R = H, Me) in the solid state (as observed in low concentration in solution; see Figure 2). Two possible pathways were investigated on the grounds of thermodynamics:[22] The addition of an extra molecule of P_4 to the known compounds **2** and **3** [Eq. (7)] and the internal disproportionation of two molecules **2**–**3** [Eq. (8)].

$$(P_4)AgAl[OC(R)(CF_3)_2]_4(s) + P_4(s) \longrightarrow [Ag(P_4)_2^+]\{Al[OC(R)(CF_3)_2]_4^-\}(s) \quad (7)$$

ΔH = 215 (R = H) and 236 kJ mol^{-1} (R = CH_3)

$$(P_4)AgAl[OC(R)(CF_3)_2]_4(s) \longrightarrow [Ag(P_4)_2^+]\{Al[OC(R)(CF_3)_2]_4^-\}(s) + Ag\{Al[OC(R)(CF_3)]_4\}(s) \quad (8)$$

ΔH = 273 (R = H) and 304 kJ mol^{-1} (R = CH_3)

Both reactions are highly unfavorable, and this accounts for the exclusive formation of **2** and **3**. Analysis of the Born–Fajans–Haber cycles for Equations (7) and (8) shows that the most unfavorable contribution for a reaction as delineated is the heterolytic gas-phase dissociation of the $(P_4)AgAl[OC(R)(CF_3)_2]_4$ (**2**, **3**) into $Ag(P_4)^+$ and $Al[OC(R)(CF_3)_2]_4^-$, which is endothermic by 415 kJ mol^{-1}.[25] The gain in lattice potential enthalpy does not compensate for this reaction enthalpy. This shows that only the most weakly coordinating anion, that is, the perfluorinated $Al[OC(CF_3)_3]_4^-$ ion, which in all silver compounds structurally characterized so far does not form Ag–O contacts,[9] is able to stabilize the $Ag(P_4)_2^+$ cation in the solid state.

*The silver–P_4 bonding in **1**–**3***: In general, linear twofold coordination is the electronically and electrostatically preferred coordination mode of the Ag^+ ion towards a variety of soft C-, N-, P-, and S-donor ligands (e.g., CN^-, SCN^-, NH_3).[26] The coordination of Ag^+ by strongly electronegative O and F ligands is unfavorable and, if enforced, results in higher coordination numbers (CN) of 4–9 with many weak electrostatic Ag–O and Ag–F contacts that adopt positions on a sphere around the silver ions.[9] Between these two extremes lies the bonding situation in **1**–**3**. In contrast to NH_3, tetrahedral white phosphorus is a very weak base (the proton affinity is only 748 kJ mol^{-1}; cf. 847 kJ mol^{-1} for NH_3[27]), and only if the counterion is sufficiently less basic than P_4 a Lewis acid–base complex is formed. However, as seen for the Li^+ cation above, this electrostatic criterion is not sufficient to allow the isolation of an $M^+(P_4)$ complex when M^+ is a hard univalent metal like lithium. Only the use of the soft Ag^+ ion allowed for the electronic stabilization of the initial electrostatic Lewis acid–base complex. This may be seen from the similar energies of the LUMO of the Ag^+ ion at −0.206 a.u. ($5s^0$ orbital) and the HOMO of the P_4 molecule (−0.370 a.u.[28]). In this respect the bonding in the $Ag(\eta^2\text{-}P_4)$ moieties is similar to that of $Ag(\eta^2\text{-}C_2H_4)^+$ units, and the $Ag(P_4)_2^+$ cation may be viewed as a mainly electrostatic complex of an Ag^+ ion with linear coordination of two electron pairs of the two-coordinate P–P bonds. However, if electrostatic interactions were the only contribution to the bonding, one would expect a tetrahedral arrangement of the two coordinated P–P edges (i.e., structure **4b**), as was observed in D_{2d}-symmetric $Pd(\eta^2\text{-}H_2)_2$ with the isolectronic neutral $4d^{10}$ Pd^0 atom.[29] The observed planar conformation of $Ag(P_4)_2^+$ (**4a**) suggested additional d-orbital contributions to the $Ag(\eta^2\text{-}P_4)$ bonding (backbonding), and indeed, inspection of the calculated molecular orbitals of **4a** suggested that the planar conformation may be induced by $d_{x^2-y^2}(Ag) \rightarrow \sigma^*(P\text{–}P)$ back bonding. The filled $d_{x^2-y^2}$ orbital of the Ag^+ ion donates electron density into the empty σ* orbital of the coordinated P–P bond of the P_4 tetrahedron (Figure 12).

The three orbitals [1 $d_{x^2-y^2}$ and 2 σ*(P–P)] transform into one bonding (b.), one nonbonding (n.b.), and one antibonding

  0947-6539/02/0803-0706 $ 17.50+.50/0 *Chem. Eur. J.* **2002**, *8*, No. 3

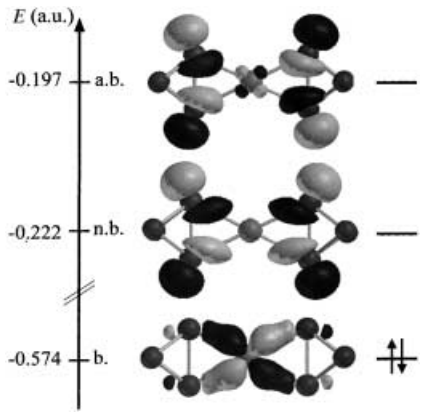

Figure 12. $d_{x^2-y^2}(Ag) \rightarrow \sigma^*(P-P)$ interaction in $Ag(P_4)_2^+$.

(a.b.) molecular orbital, only the bonding combination of which is occupied. In principle a similar interaction should also be feasible in a tetrahedral ligand field, given the small energy difference between the planar (**4a**) and tetrahedral (**4b**) conformations of only 5.2 kJ mol^{-1}. The final preference for the planar conformation may be induced by the ligand field. In a planar ligand field the five degenerate atomic d orbitals transform into four sets of orbitals, the $d_{x^2-y^2}$ orbital of which is shifted to highest energy (to +12.28 Dq),[30] that is, to much higher energy than the three t_2 orbitals in a tetrahedral ligand field (to +1.78 Dq).[30] Therefore the $d_{x^2-y^2}$ orbital of the Ag^+ ion of $Ag(P_4)_2^+$ (**4a**) lies at sufficiently high energy to interact with the empty σ* orbital of the coordinated P–P bond, as shown in Figure 12. Moreover, only one d orbital is at high energy (the energetically closest d_{xy} orbital lies at a much lower energy of +2.28 Dq[30]), which thus explains the planar arrangement. A natural bond orbital (NBO) analysis assigns a stabilization energy of 41 kJ mol^{-1} to this process. However, as can be seen from the small energy difference between planar **4a** and tetrahedral **4b** of 5.2 kJ mol^{-1}, the additional electronic stabilization achieved by a planar arrangement of the ligands is small. However in both isomers **4a** and **4b** an unusual polarization of the closed $4d^{10}$ shell of the silver atom occurs. This is due to backbonding from the silver atom to the positively charged phosphorus atoms. With this process the unfavorable positive charge residing on the coordinated phosphorus atoms[31] is removed, and the partial charges of P_{coord} are now −0.06 (Mulliken) or −0.10 (NBO).

Another unusual planar coordination environment of the Ag atom was observed in the neutral D_{2h} complex $Ag^0(C_2H_4)_2$ (matrix-isolation ESR[32]). Since a significant amount of the positive charge of the Ag^+ ion in **1** was transferred to the $P_{noncoord}$ atoms (see solid-state contacts and calculated charges of +0.16 (NBO) to +0.17 (Mulliken)), the Ag atom in $Ag(P_4)_2^+$ presumably has a similar electronic situation as that in the $Ag^0(C_2H_4)_2$ molecule, and therefore a similar planar bonding situation resulted. Moreover, the complex of the weak Lewis base dicyanogen with $AgAsF_6$ also exhibits planar coordination of the Ag^+ atom.[33] In d^{10} $Pd^0(\eta^2\text{-}H_2)_2$ the tetrahedral D_{2d} arrangement of the two H_2 moieties is only very slightly preferred over the planar D_{2h} form.[34]

Let us now examine the situation for compounds **2** and **3**, in which a tetrahedral (**2**) and a (to a first approximation) planar (**3**) coordination environment of the Ag atom are realized. As shown above in the thermodynamics section, the more basic anions interact more strongly with the silver atom than an additional P_4 molecule. The nature of this Ag–O interaction is more electrostatic and therefore the tetrahedral conformation, as in **2** (or **6a**), is expected to be the most stable on electrostatic grounds. This shows that the planar local AgO_2P_2 coordination environment in **3** is enforced by the head-to-tail dimerization of the two $(P_4)AgAl[OC(H)(CF_3)_2]_4$ units that finally leads to an elongated octahedral coordination sphere around the Ag atoms in **3** if the weak Ag–P and Ag–F contacts at 3.25 to 3.43 Å are included. Consistently, the planar species **6b** lies only 15 kJ mol^{-1} higher in energy than the tetrahedral species **6a**.

Atoms in molecules (AIM) and natural bond orbital *(NBO) analyses of $Ag(P_4)_2^+$ and $[RhCl(P_4)(PH_3)_2]$*: To compare the η^2-P_4 bonding situation in **1**–**3** and $[RhCl(P_4)(PPh_3)_2]$ and to investigate the question whether the coordinated edge of the P_4 moiety in **1**–**3** or the rhodium compound must be regarded as a P–P bond or not, AIM and NBO population analyses[35, 44] were performed for $Ag(P_4)_2^+$ and $[RhCl(P_4)(PH_3)_2]$ with the correlated MPW1PW91 electron density. For comparison the $Ag(C_2H_4)^+$ ion was also analyzed.[36] Table 4 summarizes the results of the population analyses; the calculated bond paths and bond critical points (BCPs) for both species are shown in Figure 13.

Table 4. Electron densities ρ residing on the BCPs, calculated natural charges q and Wiberg bond orders *b.o.* of P_4, $Ag(P_4)_2^+$, $[RhCl(P_4)(PH_3)_2]$, and $Ag(C_2H_4)^+$.

Property	P_4	$Ag(P_4)_2^+$	$[RhCl(P_4)(PH_3)_2]$	$Ag(C_2H_4)^+$
$\rho(P-P_{noncoord})$ [e Å^3]	0.112	0.099–0.106	0.110–0.111	–
$\rho(P-P_{coord})$ [e Å^3]	–	0.078	–	0.319[a]
$\rho(M-P_{coord})$ [e Å^3]	–	0.046	0.096	0.058[b]
q(M)	–	+0.74	+0.08	+0.93
$q(P_{coord})$	–	−0.10	−0.04	+0.04[c]
$q(P_{noncoord})$	–	+0.16	−0.01	–
b.o.$(P-P_{coord})$	–	0.90	0.48	1.83[d]
b.o.$(P-P_{noncoord})$		0.99	0.95–0.99	–
b.o.$(M-P_{coord})$	–	0.18	0.60	0.20

[a] $\rho(C-C_{coord})$. [b] $\rho(M-C_{coord})$. [c] $q(C_{coord})$ with q(H) summed into q(C). [d] *b.o.*$(C-C_{coord})$.

Figure 13 shows that the coordinated P–P edge incorporates a P–P BCP in $Ag(P_4)_2^+$ (**4a**) but not in $[RhCl(P_4)(PH_3)_2]$ (**10**). This implies the breaking of one covalent P–P bond in **10** with formation of two new covalent Rh–P bonds in keeping with the calculated electron density residing on the Rh–P BCPs (0.096 e Å^3 versus only 0.046 e Å^3 on the Ag–P BCP and about 0.10–0.11 e Å^3 on the P–P BCPs) and the highly endothermic dissociation of **10** into **11** and P_4. In contrast, the coordination of the P_4 molecules in **1**–**3** is very weak, and the presence of an AIM BCP on the coordinated P–P edge of **4a** (0.078 e Å^3, cf. 0.099–0.106 on the other P–P bonds) shows that this edge is a slightly weakened P–P bond. A similar conclusion was drawn from the NBO analysis: The Wiberg bond order of the uncoordinated P–P edges in both **4a** and **10** ranges from 0.95 to 0.99. In **4a** the coordinated P–P bond has a bond order of 0.90, but in **10** this bond order is reduced to

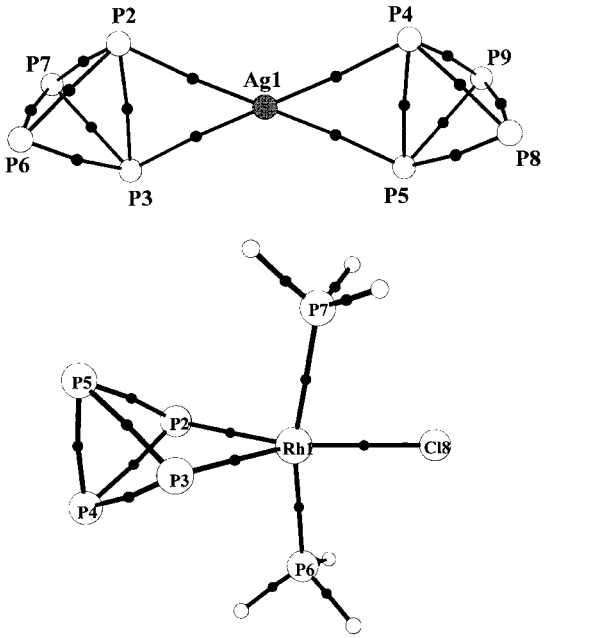

Figure 13. Calculated AIM bond paths and BCPs (●) of $Ag(P_4)_2^+$ (**4a**) and $[RhCl(P_4)(PH_3)_2]$ (**10**).

only 0.48 while the M–P bond order increases from 0.18 (M = Ag) to 0.60 (M = Rh). In contrast to **4a**, the M–P bond order in **10** is higher than the b.o. of the coordinated P–P edge. From the NBO and AIM analyses it therefore follows that the P_4 moiety in **10**, and hence also that in $[RhCl(P_4)(PPh_3)_2]$[4b], is best described as being formally derived from P_4^{2-} in a tetraphosphabicyclobutane structure rather than from a neutral tetrahedral P_4 molecule, and neither **10** nor $[RhCl(P_4)(PPh_3)_2]$ contains intact tetrahedral P_4 molecules and each has covalent Rh–P bonds. Compounds **1**–**3** are the first compounds that contain a side-on coordinated tetrahedral P_4 molecule. Strong support for this interpretation is found in sections of the calculated total electron densities[37] of neutral P_4 (Figure 14a), $Ag(P_4)_2^+$ (**4a**; Figure 14b), and $[RhCl(P_4)(PH_3)_2]$ (**10**; Figure 14c).

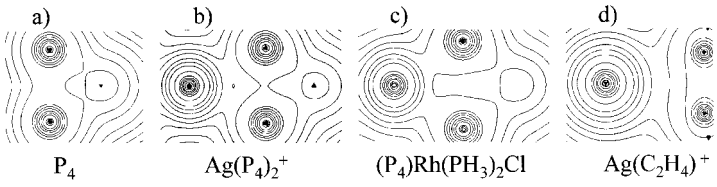

Figure 14. Sections of the calculated total electron densities[37] of neutral P_4 through the P–P bond (a), $Ag(P_4)_2^+$ **4a** through the AgP_2 plane (b), $[RhCl(P_4)(PH_3)_2]$ (**10**) through the RhP_2 plane (c) and $Ag(C_2H_4)^+$ through the AgC_2 plane (d).

The topology of the total electron density of the P–P bond in free P_4 is only slightly distorted when coordinated to Ag^+ (Figure 14a, b), and the center of the AgP_2 plane contains an electron-density minimum which can only be explained by backbonding in addition to the electrostatic coordination of the P–P bonds. The topology of the total electron density of the RhP_2 plane in **10** is in sharp contrast to those of P_4 and $Ag(P_4)_2^+$, and the curvature of the RhP_2 electron density suggests the presence of covalent Rh–P bonds but only weak interactions between the two P atoms of the coordinated P–P edge.

A comparison of the bonding in $Ag(P_4)_2^+$ and $Ag(C_2H_4)^+$ reveals distinct differences: the AIM analysis of $Ag(C_2H_4)^+$ (MP2 level) gave only two BCPs residing on the C–C bond and on the line between the Ag atom and the center of the C–C bond[38] (no ring point was found, in contrast to **4a**). This curvature of the electron density was interpreted[38] as arising from an interaction of the π electrons of C_2H_4 with the Ag^+ ion to give a T-shaped, mainly electrostatic bonding with little or no backbonding from the occupied 4d orbitals of Ag^+. Consequently, the topology of the total electron density of $Ag(C_2H_4)^+$, calculated at the same level as those of P_4, $Ag(P_4)_2^+$, and $[RhCl(P_4)(PH_3)_2]$,[37] (Figure 14d) is very different to those shown in Figure 14b and c. This is also seen in the calculated natural charges (Table 4) residing on the silver atom in **4a** (+0.74) and $Ag(C_2H_4)^+$ (+0.93). In **4a** the positive charge is more highly delocalized by backbonding than in $Ag(C_2H_4)^+$, and therefore the positive partial charge residing on the silver atom in **4a** is smaller than in $Ag(C_2H_4)^+$ by 0.19.

Conclusion

We have shown: 1) By employing very weakly coordinating anions of the type $Al[OC(CF_3)_2(R)]_4^-$ (R = H, CH_3, CF_3) superweak complexes of the Ag^+ ion and the tetrahedral P_4 molecule can be synthesized. The unusual D_{2h}-symmetric $Ag(P_4)_2^+$ ion is only stable with the most weakly coordinating $Al[OC(CF_3)_3]_4^-$ spectator anion. Addition of weak bases like benzene or COD decomposes the $Ag(P_4)_2^+$ complex. 2) The bonding of the Rh(η^2-P_4) moiety in $[RhCl(P_4)(PPh_3)_2]$ compound[4b] should be reassigned as formally being derived from Rh^{III} and P_4^{2-} in a tetraphosphabicyclobutane structure with two covalent Rh–P bonds but very little P–P bonding in the coordinated P–P edge of the Rh(η^2-P_4) substructure. Therefore, **1**–**3** are the first unambiguously characterized compounds with side-on η^2-coordinated tetrahedral P_4 molecules. 3) To a first approximation the Ag atom in $Ag(P_4)_2^+$ is linearly coordinated by the two electron pairs of the two coordinated P–P bonds to give a mainly electrostatic complex. The final small preference for the planar coordination environment of the Ag atom is mediated by an unusual backbonding [$d_{x^2-y^2}$(Ag) → σ*(P–P)] from the closed $4d^{10}$ shell of silver, which minimizes the unfavorable positive charge on the phosphorus atoms. This shows that nonclassical and weak bonding modes in weak cationic Lewis acid–base complexes can be stabilized by minimizing the electrostatic cation–anion interaction between the species. Similarly, large and weakly basic anions such as $Al[OC(CF_3)_3]_4^-$[9] will be useful for designing a variety of compounds in which cation–anion interaction should be minimized, for example, in homogenous catalysis, for highly electrophilic and/or oxidizing cations, and elsewhere.

Currently we are investigating the reactivity of these Ag–P_4 complexes towards oxidizing agents such as the halogens.[39, 40]

0947-6539/02/0803-0708 $ 17.50+.50/0 *Chem. Eur. J.* **2002**, *8*, No. 3

Experimental Section

All manipulations were performed by using standard grease-free Schlenk or dry-box techniques and a dinitrogen or argon atmosphere. Apparatus were closed by Young valves. All solvents were rigorously dried and degassed prior to use and stored under N_2. Yellow phosphorus was sublimed prior to use and dissolved in CH_2Cl_2 or CS_2 to give stock solutions which were manipulated by syringe techniques. The silver aluminates $Ag[Al(OR_F)_4]$ were prepared according to the literature.[9] Raman spectra were obtained from solid samples sealed in a melting point capillary or a 5 mm NMR tube. NMR spectra of sealed samples were recorded in CD_2Cl_2 and were referenced to the solvent (^1H, ^{13}C) or external H_3PO_4 (^{31}P) and aqueous $AlCl_3$ (^{27}Al). Solid-state NMR experiments for **1** were performed on a Bruker DSX 400 spectrometer operating at 9.4 T, corresponding to a ^{31}P frequency of 162 MHz. A 7 mm MAS probe allowing variable temperature measurements in the range of 150–573 K was used. MAS was performed at 3 kHz.

$[Ag(P_4)_2]\{Al[OC(CF_3)_3]_4\}$ (1): A solution of P_4 in CS_2 (4.57 mL, 1.566 M, 7.152 mmol) was added to solid $Ag(CH_2Cl_2)Al[OC(CF_3)_3]_4$ (4.148 g, 3.576 mmol) at room temperature. The resulting suspension was dissolved by addition of CH_2Cl_2 (10 mL) to give a clear colorless solution over a little dark brown precipitate. After the dark material had settled (ca. 2 h), the mixture was filtered through a fine glass frit, and all volatile matter removed in vaccuo to leave a beige microcrystalline and pyrophoric material (3.984 g, 84 %). Crystals of **1** suitable for X-ray crystallography were obtained by recrystallization of part of the highly soluble beige material from CH_2Cl_2 (ca. 0.5 mL). The crystals decompose above 100 °C with darkening; a Raman spectrum of this material after determination of the decomposition point showed no bands. ^{13}C NMR (63 MHz, CD_2Cl_2, 25 °C): $\delta = 121.6$ (q, $J_{C,F} = 293.1$ Hz; CF_3); ^{27}Al NMR (78 MHz, CD_2Cl_2, 25 °C): $\delta = 36.0$ (s, $\nu_{1/2} = 14$ Hz), ^{31}P NMR (101 MHz, CD_2Cl_2, 25 °C): $\delta = -497$ (s, P_4, $\nu_{1/2} = 25$ Hz); ^{31}P NMR (101 MHz, CD_2Cl_2, −100 °C): $\delta = -486$ (s, P_4, $\nu_{1/2} = 220$ Hz); FT-Raman: $\tilde{\nu}(\%) = 798$ (7, Al–O), 746 (7, Al–O), 601 (100, P_4-A_g), 473 (18, P_4-B_{2g}), 458 (16, P_4-B_{1g}), 413 (5, P_4-A_g), 381 (sh, P_4-B_{3g}), 374 (9, P_4-A_g), 322 cm^{-1} (5, Al–O).

$Ag(P_4)Al[OC(CH_3)(CF_3)_2]_4$ (2): A solution of P_4 in CH_2Cl_2 (38.8 mL, 0.06 M, 2.330 mmol) was added to solid $Ag(CH_2Cl_2)Al[OC(CH_3)(CF_3)_2]_4$ (2.200 g, 2.330 mmol) at room temperature. After 1 h the resulting solution over a little dark brown precipitate was filtered through a fine glass frit, and all volatile matter was removed in vaccuo to leave a beige microcrystalline and pyrophoric material (1.786 g, 78 %). Crystals of **3** suitable for X-ray crystallography were obtained by recrystallization of part of the highly soluble beige material from CH_2Cl_2 (ca. 0.5 mL) (m.p. 80–85 °C, some decomposition starting at about 70 °C). ^1H NMR (250 MHz, CD_2Cl_2, 25 °C): $\delta = 1.59$ (s, CH_3); ^{13}C NMR (63 MHz, CD_2Cl_2, 25 °C): $\delta = 18.0$ (s, CH_3), 76.3 (sept, $^2J_{C,F} = 29.8$ Hz), 124.0 (q, $^1J_{C,F} = 288.4$ Hz; CF_3); ^{27}Al NMR (78 MHz, CD_2Cl_2, 25 °C): $\delta = 45.9$ (s, $\nu_{1/2} = 310$ Hz); ^{31}P NMR (101 MHz, CD_2Cl_2, 25 °C): $\delta = -515$ (s, P_4, $\nu_{1/2} = 32$ Hz); ^{31}P NMR (101 MHz, CD_2Cl_2, −100 °C): $\delta = -466$ (br, 1P), −518 (br, 7P); FT-Raman: $\tilde{\nu}(\%) = 2964$ (8, CH_3), 772 (6, Al–O), 598 (100, P_4-A_1), 469 (sh, P_4-B_1), 457 (29, P_4-B_2), 414 (7, P_4-A_1), 375 (6, P_4-A_2), 358 (6, P_4-A_1), 331 cm^{-1} (4, Al–O); elemental analysis (%) calcd for $AgAlO_4P_4C_{16}H_{12}F_{24}$ (983.00): Al 2.74, P 12.60; found: Al 2.59, P 12.02.

$[\{Ag(P_4)Al[OC(H)(CF_3)_2]_4\}_2]$ (3): Solid $AgAl[OC(H)(CF_3)_2]_4$ (7.483 g, 9.319 mmol) was suspended in 20 mL of pentane and a solution of P_4 in CS_2 (5.95 mL, 1.566 M, 9.319 mmol) was added at room temperature. The resulting clear colorless solution over a little dark brown precipitate was filtered through a fine glass frit, and all volatile matter was removed in vacuo to leave a slightly brown clear oil which solidified on standing overnight at 0 °C as a beige microcrystalline material (7.386 g, 86 %). Crystals of **2** suitable for X-ray crystallography were obtained by recrystallization of part of the beige material from pentane (ca. 5 mL) (m.p. 46–51 °C). ^1H NMR (250 MHz, CD_2Cl_2, 25 °C): $\delta = 4.54$ (sept, $^3J_{H,F} = 5.6$ Hz); ^{13}C NMR (63 MHz, CD_2Cl_2, 25 °C): $\delta = 70.9$ (sept, $^2J_{C,F} = 33.1$ Hz), 122.5 (q, CF_3, $^1J_{C,F} = 285.8$ Hz); ^{27}Al NMR (78 MHz, CD_2Cl_2, 25 °C): $\delta = 57.0$ (s, $\nu_{1/2} = 280$ Hz), ^{31}P NMR (101 MHz, CD_2Cl_2, 25 °C): $\delta = -514$ (s, P_4, $\nu_{1/2} = 5$ Hz); ^{31}P NMR (101 MHz, CD_2Cl_2, −100 °C): $\delta = -504$ (s, P_4, $\nu_{1/2} = 9$ Hz); FT-Raman: $\tilde{\nu}(\%) = 856$ (6, Al–O), 765 (5, Al–O), 598 (100, P_4-A_1), 471 (26, P_4-B_1, P_4-B_2), 414 (8, P_4-A_1), 374 (12, P_4-A_1, P_4-A_2), 331 cm^{-1} (4, Al–O).

Reaction of 1 with 1,5-cyclooctadiene: Compound **1** (0.149 g, 0.113 mmol) was weighed into an NMR tube and dissolved at room temperature in $CDCl_3$ (1.0 mL). COD (0.028 mL, 0.226 mmol) was added to the solution by syringe to give a clear, slightly brownish solution. ^1H NMR (250 MHz, $CDCl_3$, 25 °C): $\delta = 2.59$ (s, 8H; COD), 6.24 (s, 4H; COD); ^{13}C NMR

Table 5. Crystallographic and refinement details of **1**–**3**.

Compound	**1**	**2**	**3**
crystal size [mm]	0.5 × 0.5 × 0.2	0.5 × 0.5 × 0.4	0.4 × 0.3 × 0.2
crystal system	monoclinic	monoclinic	triclinic
space group	$P2_1/n$	$P2_1/n$	$P\bar{1}$
a [Å]	14.455(3)	10.563(2)	10.353(2)
b [Å]	17.385(4)	10.249(2)	17.202(3)
c [Å]	15.693(3)	29.059(6)	17.857(4)
α [°]	90	90	108.43(3)
β [°]	100.88(3)	95.16(3)	95.69(3)
γ [°]	90	90	106.50(3)
V [Å^3]	3872.8(13)	3284.6(11)	2829.8(10)
Z	4	4	2
ρ_{calcd} [Mg m^{-3}]	2.269	2.084	2.176
μ [mm^{-1}]	1.078	1.045	1.150
abs. corr.	numerical	numerical	numerical
$I_{min}/I_{max.}$	0.752/0.861	0.602/0.731	0.694/0.762
$F(000)$	2528	1904	1776
index range	$-17 < h < 17$, $0 < k < 21$, $0 < l < 19$	$-12 < h < 12$, $0 < k < 12$, $0 < l < 35$	$-11 < h < 12$, $-21 < k < 21$, $-19 < l < 21$
2θ [°]	51.76	51.80	51.86
T [K]	150	150	180
refl. unique	7202	5755	10213
refl. obs. (4σ)	4102	4911	7026
no. variables	697	454	829
weighting scheme[a] x	0.1053	0.0551	0.0555
GOOF	0.858	1.060	0.909
final R (4σ)	0.0569	0.0274	0.0369
final $wR2$	0.1572	0.0780	0.0935
larg. res. peak [e Å^3]	1.161	0.540	0.676

[a] $w^{-1} = \sigma^2 F_o^2 + (xP)^2$; $P = (F_o^2 + 2F_c^2)/3$.

(63 MHz, $CDCl_3$, 25 °C): $\delta = 27.9$ (COD), 121.3 (q, $^1J_{C,F} = 292.9$ Hz; CF_3), 127.6 (COD); ^{31}P NMR (101 MHz, $CDCl_3$, 25 °C): $\delta = -521$ (s, P_4, $\nu_{1/2} = 4$ Hz).

Reaction of 1 with S_8: Compound **1** (0.151 g, 0.114 mmol) and S_8 (0.058 g, 0.228 mmol) were weighed into a NMR tube and dissolved at room temperature in $CDCl_3$ (1.0 mL) to give a clear, slightly brownish solution over a yellowish solid material that appeared to be unconsumed sulfur. The sealed NMR tube was exposed for 30 min to ultrasound which resulted in no visible change of the reaction mixture. ^{31}P NMR (101 MHz, $CDCl_3$, 25 °C): $\delta = -496$ (s, $Ag(P_4)_2^+$, $\nu_{1/2} = 8$ Hz).

X-ray crystal structure determinations: Data for X-ray structure determinations were collected on a STOE IPDS diffractometer with graphite-monochromated $Mo_{K\alpha}$ radiation ($\lambda = 0.71073$ Å). Single crystals were mounted in perfluoroether oil on top of a glass fiber and then brought into the cold stream of a low-temperature device so that the oil solidified. All calculations were performed on PCs using the Siemens SHELX93 software package. The structures were solved by the Patterson heavy atom method and successive interpretation of the difference Fourier maps, followed by least-squares refinement. All non-hydrogen atoms were refined anisotropically. The hydrogen atoms were included in the refinement in calculated positions by a riding model using fixed isotropic parameters. Relevant data concerning crystallography, data collection, and refinement details are compiled in Table 5. Crystallographic data (excluding structure factors) for the structures reported in this paper have been deposited with the Cambridge Crystallographic Data Centre as supplementary publication nos. CCDC-141492 (**1**), CCDC-158942 (**2**), and CCDC-158943 (**3**). Copies of the data can be obtained free of charge on application to CCDC, 12 Union Road, Cambridge CB21EZ, UK (fax: (+44) 1223-336-033; e-mail: deposit@ccdc.cam.ac.uk).

Methods of calculation: All calculations were performed with the Gaussian 98W[41] suite of programs. The geometries of **4–11** were optimized at the hybrid HF-DFT MPW1PW91/TZV(df) level.[42, 43] For silver and rhodium we used the standard 3–21G(d) basis set augmented with one set of diffuse and f-polarization functions each [3-21 + G(df)]. Isotropic NMR shielding tensors of **4** and **5** were calculated by the GIAO method using MPW1PW91 and the same basis sets as above. ^{31}P NMR shifts were obtained by comparison to the calculated isotropic shielding tensor of P_4 ($\delta = 858.8$) and its experimental shift at $\delta(^{31}P) = -522$. Approximate solvation energies (CH_2Cl_2 solution with $\varepsilon_r = 8.92$) were calculated with the COSMO model at the BP86/3-21G* level. Frequency calculations were performed for all species and, unless otherwise stated, the structures represent true minima without imaginary frequencies on the respective hypersurface. For thermodynamic calculations the zero-point energy and thermal contributions to the enthalpy and the free energy at 298 K were included. For selected species an AIM[44] or NBO population analysis[35] was performed with the MPW1PW91/TZV(df) electron density.

Acknowledgement

We thank Prof. H. Schnöckel for valuable discussions and advice and Dipl.-Chem. G. Stösser and Dipl.-Chem. J. Bahlo for recording the Raman spectra. Financial support from the Deutsche Forschungsgemeinschaft and a Liebig grant from the Fonds der Chemischen Industrie are gratefully acknowledged.

[1] J. L. Abboud, M. Herreros, R. Notario, M. Esseffar, O. Mo, M. Yanez, *J. Am. Chem. Soc.* **1996**, *118*, 1126.
[2] J. L. Abboud, I. Alkorta, J. L. Davalos, J.-F. Gal, M. Herreros, P.-C. Maria, O. Mo, M. T. Molina, R. Notario, M. Yanez *J. Am. Chem. Soc.* **2000**, *122*, 4451.
[3] M. Lin, C. Liu, L. Zheng, *Wuli Huaxue Xuebao* **1995**, *11*, 266.
[4] a) M. D. Vaira, L. Sacconi, *Angew. Chem.* **1982**, *94*, 338; *Angew. Chem. Int. Ed. Engl.* **1982**, *21*, 330; b) A. P. Ginsberg, W. F. Lindsell, K. J. McCullough, C. R. Sprinkle, A. J. Welsh, *J. Am. Chem. Soc.* **1986**, *108*, 403–416; c) T. Göer, G. Baum, M. Scheer, *Organometallics* **1998**, *17*, 5916; d) M. Peruzzini, L. Marvelli, A. Romerosa, R. Bossi, F. Vizza, F. Zanobini, *Eur. J. Inorg. Chem.* **1999**, 931.
[5] O. J. Scherer, *Chem. unserer Zeit* **2000**, 374.
[6] a) M. Scheer, E. Herrmann, *Z. Chem.* **1990**, *29*, 41; b) O. J. Scherer, *Angew. Chem.* **1990**, *102*, 1137; *Angew. Chem. Int. Ed. Engl.* **1990**, *29*, 1104; c) K. H. Whitmire, *Adv. Organomet. Chem.* **1998**, *42*, 2.
[7] However, earlier investigations showed that the final product of the reaction of silver salts with P_4 is Ag_3P: O. J. Walker, *J. Chem. Soc.* **1926**, 1370.
[8] I. Krossing, *J. Am. Chem. Soc.* **2001**, *123*, 4603.
[9] I. Krossing, *Chem. Eur. J.* **2001**, *7*, 490.
[10] T. S. Cameron, A. Decken, I. Krossing, J. Passmore, unpublished results.
[11] These exchange processes and the small gyromagnetic ratio of the NMR-active ^{107}Ag ($I = 1/2$, ca. 50% natural abundance) and ^{109}Ag ($I = 1/2$, ca. 50% natural abundance) nuclei presumably preclude the observation of Ag–P coupling.
[12] To compensate for the highly temperature and concentration dependent ^{31}P NMR shift of the free P_4 molecule in CD_2Cl_2, a sample of P_4 in CD_2Cl_2 with approximately the same concentration as in the $Ag^+ - P_4$ mixtures (about 0.1M) was prepared and run under the same conditions as the silver-containing samples. In all the prepared Ag–P_4 samples at all tested temperatures (25, −40, −60, −80 °C) no evidence was found for new $Ag(P_4)_x^+$ ions, nor could Ag–P coupling be resolved. However, it was noted that solid P_4 precipitated from the Ag–P_4 samples upon cooling and appeared in the NMR spectra as a broad signal at $\delta(^{31}P) \approx -455 \pm 3$. The same broad signal of characteristic shape ($h_{1/2} = 2000$ Hz, solid P_4, cf. ^{31}P MAS-NMR of P_4: $\delta = -461$) was observed when the CD_2Cl_2 solution of (not very soluble) P_4 was measured at low temperatures. Solid P_4 has a cubic crystal lattice in which the P_4 molecule maintains its local T_d symmetry. Due to this highly symmetric environment of the solid P_4 molecule the dipole–dipole interactions that usually lead to very broad signals for solid samples (without magic angle spinning) cancel, and one observes a relatively sharp signal for solid precipitated P_4 even on a conventional NMR spectrometer. In the pure P_4/CD_2Cl_2 sample, a second sharp signal for free dissolved P_4 remained visible beside the broad line of solid P_4 at all temperatures down to −80 °C. The ^{31}P-NMR shifts of pure dissolved P_4 in CD_2Cl_2 are: −522.3 at 25 °C, −518.7 at −40, −517.3 at −60, and −516.0 at −80 °C.
[13] In **2** the electron deficiency of the Ag^+ ion is more highly saturated by two Ag–O contacts to the more electron rich $OC(CH_3)(CF_3)_2$ ligand. Therefore the electrostatic contribution to the Ag–P bonding is smaller, and the P_4 molecules in **2** are more weakly bound than those in **1** and **3** with less basic anions. The weakest coordination of the P_4 molecule in **2** is also evident from the bond lengths of the coordinated P–P edge, which follow the order **1** > **3** > **2** or 2.329(2) > 2.326(2) > 2.308(1) Å.
[14] Z. Xu, B.-M. Wu, T. C. W. Mak, J. Manning, C. A. Reed, *J. Chem. Soc. Dalton Trans.* **1997**, 1213, and references therein.
[15] A. Albinati, S. V. Meille, G. J. Carturan, *J. Organomet. Chem.* **1979**, *182*, 269.
[16] I. Krossing, unpublished results.
[17] At 200 K the lattice parameters of **1** are $a = 9.704(2)$, $b = 17.408(3)$, $c = 11.683(2)$ Å, monoclinic crystal system, $\beta = 94.78(3)°$, $V = 1966.7$ Å^3. A full data set with 15353 reflections (unique: 7458, observed ($I > 4\sigma(I)$): 5776, $R_{int} = 0.046$, $-11 < h < 11$, $-21 < k < 21$, $-13 < l < 14$, max. $2\theta = 51.90°$) was collected on a STOE IPDS diffractometer. The structure solution and refinement led to final agreement factors of $R1 = 0.1187$ ($I > 4\sigma$) (0.1384 for all data) and $wR2 = 0.3643$, GOF 1.183. Selected bond lengths [Å] and angles [°]: Ag1–P5 2.536(4), Ag1–P6 2.543(4) Ag1–P1 2.544(4), Ag1–P2 2.550(4), P1–P2 2.307(5), P5–P6 2.335(5), P1–P3 2.085(6), P1–P4 2.131(6), P2–P3 2.169(6), P2–P4 2.168(7), P5–P7 2.172(7), P5–P8 2.129(6), P6–P7 2.132(7), P6–P8 2.163(6), P3–P4 2.106(6), P7–P8 2.183(7); P5-Ag1-P6 54.7(1), P5-Ag1-P1 176.6(1), P5-Ag1-P2 126.7(1), P6-Ag1-P1 124.6(1), P6-Ag1-P2 177.8(1), P1-Ag1-P2 53.8(1).
[18] a) M. Di Vaira, P. Stoppioni, M. Peruzzini, *J. Chem. Soc. Dalton Trans.* **1990**, 109; b) M. Di Vaira, M. P. Ehses, M. Peruzzini, P. Stoppioni, *Polyhedron* **1999**, *18*, 2331.
[19] P. K. Hurlburt, O. P. Anderson, S. H. Strauss, *J. Am. Chem. Soc.* **1991**, *113*, 6277.
[20] Scaling factors f were derived by comparison of the calculated frequencies of P_4 to the experimentally observed values. For the A_1 mode $f = 1.026$, for the T_2 mode $f = 0.986$, and for the E mode $f = 0.967$.

  0947-6539/02/0803-0710 $ 17.50+.50/0 *Chem. Eur. J.* **2002**, *8*, No. 3

[21] H. K. Roobottom, H. D. B. Jenkins, J. Passmore, L. Glasser, *Inorg. Chem.* **1999**, *38*, 3609.
[22] Estimations including lattice potential enthalpies and/or sublimation enthalpies are naturally less accurate than gas-phase calculations performed with hybrid HF/DFT methods. However, usually error cancellation occurs and, if used consistently, the resulting reaction enthalpies are correct to about $\pm 30\,kJ\,mol^{-1}$. For detailed examples and discussions of these thermochemical estimations, see S. Brownridge, I. Krossing, J. Passmore, H. D. B. Jenkins, H. K. Roobottom, *Coord. Chem. Rev.* **2000**, *197*, 397.
[23] It is not possible to directly establish the quality of the calculated data, since experimental determinations of either reaction or formation enthalpies of gaseous Ag^+-P_4 complexes are not available in the literature. However, the dissociation enthalpy of $Ag(C_2H_4)^+$ into Ag^+ and C_2H_4 was determined to be $141\,kJ\,mol^{-1}$, and our calculation gave a value of $156\,kJ\,mol^{-1}$. This can be compared to the BP86, B3LYP, MP2, and CCSD(T) values given in ref. [38], which range from 134 to $171\,kJ\,mol^{-1}$. Another test is the calculation of the dimerization of P_2 to give $0.5\,P_4$, which is exothermic by $114\,kJ\,mol^{-1}$, by using the standard enthalpies of formation provided in *Handbook of Chemistry and Physics*, 80th edition, (Ed.: D. R. Lide), CRC Press, Boca Raton, **1999**. Our calculation at the MPW1PW91/TZV(df) level gave a similar value of $94\,kJ\,mol^{-1}$.
[24] The complete fragmentation of $Ag(P_4)_2^+$ (**4a**) into Ag^+ and $2\,P_4$ is endothermic (endergonic) by 265 (186) $kJ\,mol^{-1}$.
[25] As an approximation of this gas-phase dissociation of **1** and **2** we used the calculated dissociation enthalpy of **6a** into **5** and **8** .
[26] One usually assumes a linear $5s4d_z^2$ hybridization of the Ag^+ ion that is favored by the relativistic orbital contraction of the 5s orbital; see P. Schwerdtfeger, P. D. W. Boyd, A. K. Burrell, W. T. Robinson, M. Taylor, *Inorg. Chem.* **1990**, *29*, 3593.
[27] J. L. Abboud, M. Herreros, R. Notario, M. Esseffar, O. Mo, M. Yanez, *J. Am. Chem. Soc.* **1996**, *118*, 1126.
[28] HOMO and LUMO energies were calculated at the HF/3-21G* level for Ag^+ and P_4. In contrast to DFT, HF theory gives correct orbital ordering also for atomic calculations (as needed for Ag^+).
[29] However, also in this complex the planar D_{2h} form is only slightly less favorable; see ref. [34].
[30] *Holleman-Wiberg*, *Lehrbuch der Anorganischen Chemie*, 101st Ed., Walter de Gruyter, Berlin, **1995**, p. 1255.
[31] The capability of the phosphorus atom to bear a positive charge is very low, as shown, for example, by the many Zintl-type polyphosphorus anions but the nonexistence of naked polyphosphorus cations in condensed phases.
[32] a) P. H. Kasai, D. McLeod, T. Watanabe *J. Am. Chem. Soc.* **1980**, *102*, 179; b) P. H. Kasai *J. Phys. Chem.* **1982**, *86*, 3684.
[33] H. W. Roesky, H. Hofmann, J. Schimkowiak, P. G. Jones, K. Meyer-Bäse, G. M. Sheldrick, *Angew. Chem.* **1985**, *97*, 403; *Angew. Chem. Int. Ed. Engl.* **1985**, *24*, 417.
[34] L. Andrews, X. Wang, M. E. Alikhani, L. Manceron *J. Phys. Chem. A* **2001**, *105*, 3052.
[35] NBO Version 3.1, E. D. Glendening, A. E. Reed, J. E. Carpenter, and F. Weinhold; see J. E. Carpenter, F. Weinhold, *J. Mol. Struct. (Theochem)* **1988**, *169*, 41, and references therein.
[36] $Ag(C_2H_4)^+$ (C_{2v}) was optimized at the MPW1PW91/3-21G* level. Structural parameters and the energy of dissociation into Ag^+ and C_2H_4 are in good agreement with earlier calculations[38] (within 0.05 Å and $3\,kcal\,mol^{-1}$).
[37] Performed with the program AIM2000 using the correlated electron densities obtained from Gaussian 94W calculations at the B3PW91/3-21G* level and using the minimum structures of P_4 (T_d), $Ag(P_4)_2^+$ (D_{2h}), $[RhCl(P_4)(PH_3)_2]$ (C_s), and $Ag(C_2H_4)^+$ (C_{2v}) optimized at the same level. AIM2000 only processes wavefunction files generated by Gaussian 94W and, for consistency, this level of theory was used throughout.
[38] R. H. Hertwig, W. Koch, D. Schröder, H. Schwarz, J Hrusak, P. Schwerdtfeger, *J. Phys. Chem.* **1996**, *100*, 12253.
[39] I. Krossing, *J. Chem. Soc. Dalton Trans.* in press.
[40] I. Krossing, I. Raabe, *Angew. Chem.* **2001**, *113*, 4544; *Angew. Chem. Int. Ed.* **2001**, *40*, 4406.
[41] Gaussian 98, Revision A.3, Gaussian, Inc., Pittsburgh PA, **1998**.
[42] C. Adamo, V. Barone, *J. Chem. Phys.* **1998**, *108*, 664.
[43] a) A. Schaefer, H. Horn, R. Ahlrichs, *J. Chem. Phys.* **1992**, *97*, 2571; b) A. Schaefer, C. Huber, R. Ahlrichs, *J. Chem. Phys.* **1994**, *100*, 5829.
[44] R. F. W. Bader, *Atoms in Molecules*, Clarendon Press, Oxford, **1994**.

Received: March 7, 2001
Revised: September 12, 2001 [F3115]